Measurements of the cosmological evolution of magnetic fields with the Square Kilometre Array

Martin Krause,[1,2,3]* Paul Alexander,[1,4] Rosie Bolton,[1] Jörn Geisbüsch,[1] David A. Green[1] and Julia Riley[1]

[1]*Astrophysics Group, Cavendish Laboratory, 19 J. J. Thomson Avenue, Cambridge CB3 0HE*
[2]*Max-Planck Institut für Extraterrestrische Physik, Giessenbachstrasse, 85748 Garching, Germany*
[3]*Universitätssternwarte München, Scheinerstr. 1, 81679 München, Germany*
[4]*Kavli Institute for Cosmology Cambridge, Madingley Road, Cambridge CB3 0HA*

ABSTRACT

We investigate the potential of the Square Kilometre Array (SKA) for measuring the magnetic fields in clusters of galaxies via Faraday rotation of background polarized sources. The populations of clusters and radio sources are derived from an analytical cosmological model, combined with an extrapolation of current observational constraints. We adopt an empirical model for the Faraday screen in individual clusters, gauged to observations of nearby clusters and extrapolate the polarization properties for the radio source population from the National Radio Astronomy Observatory Very Large Array Sky Survey. We find that about 10 per cent of the sky is covered by a significant extragalactic Faraday screen. Most of it has rotation measures between 10 and 100 rad m^{-2}. We argue that the cluster centres should have up to about 5000 rad m^{-2}. We show that the proposed mid frequency aperture array of the SKA as well as the lowest band of the SKA dish array are well suited to make measurements for most of these rotation measure values, typically requiring a signal-to-noise ratio of 10. We calculate the spacing of sources forming a grid for the purpose of measuring foreground rotation measures: it reaches a spacing of 36 arcsec for a 100 h SKA observation per field. We also calculate the statistics for background rotation measure (RM) measurements in clusters of galaxies. We find that a first phase of the SKA would allow us to take stacking experiments out to high redshifts (>1), and provide improved magnetic field structure measurements for individual nearby clusters. The full SKA aperture array would be able to make very detailed magnetic field structure measurements of clusters with more than 100 background sources per cluster up to a redshift of 0.5 and more than 1000 background sources per cluster for nearby clusters, and could for reasonable assumptions about future measurements of electron densities in high-redshift clusters constrain the power-law index for the magnetic field evolution to better than $\Delta m = 0.4$, if the magnetic field in clusters should follow $B \propto (1 + z)^m$.

Key words: magnetic fields – instrumentation: polarimeters – surveys – galaxies: clusters: general – cosmology: observations – radio continuum: general.

1 INTRODUCTION

The plasma between the galaxies in clusters is magnetized. Observations at radio frequencies are our main quantitative probe of cluster magnetic fields. This is done by three main methods: equipartition arguments applied to cluster halo radio sources (e.g. Giovannini et al. 1993), comparison of X-ray inverse Compton (IC) with the radio synchrotron data in radio sources (e.g. Bagchi, Pislar & Lima Neto 1998) and Faraday rotation of polarized radio sources within or behind the cluster, combined with X-ray data to determine the electron densities (Kim, Kronberg & Tribble 1991; Clarke, Kronberg & Böhringer 2001). The results have been reviewed regularly (Carilli & Taylor 2002; Govoni & Feretti 2004; Feretti & Giovannini 2008). Galaxy clusters are found to possess magnetic fields of typically a few, up to of order 10 μG.

The structure within cluster magnetic fields has been deduced from Faraday rotation of extended cluster radio sources (Murgia et al. 2004; Vogt & Enßlin 2005; Govoni et al. 2006; Guidetti al.

*★ E-mail: M.Krause@mrao.cam.ac.uk; krause@mpe.mpg.de; mkrause@ usm.lmu.de

2008). For the few cases observed so far, the data is consistent with a Kolmogorov-type power spectrum. Because the field is frozen into the plasma in the high-conductivity limit, the structure of the field directly traces the underlying kinematics of the gas.

Current studies of magnetic fields in clusters are limited to a few nearby objects ($z < 0.1$). Hence, we have no means to answer questions regarding the origin and cosmological evolution of these fields. Correspondingly, few cosmological structure formation simulations have included magnetic fields. To date, none have the resolution to address directly the field evolution in galaxy clusters. However, from the eddy turnover times, and the high efficiency of the turbulent dynamo, one might expect that the magnetic energy should always be in equipartition with the turbulent kinetic energy (Ryu, private communication). Hence, studying the cosmological evolution of fields in clusters might not only lead to the origin of magnetism, but also trace cluster kinematics.

Magnetic fields in clusters of galaxies might be connected to the cooling flow problem. If cooling flows in nearby objects are quenched by weak jets, as has been often suggested (e.g. Kaiser & Binney 2003), the magnetic fields will be amplified up to equipartition with the enhanced kinetic energy level provided by the very same jets.

The Faraday rotation method is expected to benefit substantially from new developments of radio telescopes over the coming decade. The Australian Square Kilometre Array Pathfinder (ASKAP) project, as well as the South African Karoo Array Telescope (MEERKAT) project are expected to start operation within a few years. Both instruments will have sensitivities competitive with the enhanced Very Large Array (eVLA), but with substantially higher survey speed at frequencies below 1.4 GHz. The Square Kilometre Array (SKA) is the next generation radio interferometer and will be a transformational instrument with an improvement in sensitivity compared to the eVLA of a factor of 50 with a 10^5 increase in survey speed. At frequencies below 500 MHz, aperture arrays (AA) will form the collector with dishes at frequencies above 1.4 GHz. In the mid frequency range (0.3–1.4 GHz) large survey speeds will be achieved by using aperture arrays or dishes with focal-plane arrays (Schilizzi et al. 2007). Phase 1 of the telescope (with between 10 and 15 per cent of the collecting area) is scheduled for operation in about 2015 with phased deployment of the rest of the telescope over the next few years and with completion in 2021/22. Aperture arrays provide the most exciting technology for the mid-frequency range with the largest increase in survey speed, provided they can meet an appropriate performance to cost (Alexander & Faulkner 2009). The derived properties for the SKA, based on Schilizzi et al. (2007) and Alexander & Faulkner (2009) are summarized in Table 1, together with a comparison to the VLA.

In this paper, we investigate the potential of these instruments, in particular the SKA, to measure cosmological evolution in cluster magnetic fields. We concentrate on Faraday rotation studies: the magnetic field along the line of sight rotates the polarization angle by

$$\Delta \chi = \frac{\text{RM}}{(1+z)^2} \lambda^2, \tag{1}$$

where λ is the observing wavelength and we included the cosmological factor (z is the redshift of the rotating Faraday screen) to account for the redshift of the radio emission travelling from the Faraday screen to us. This factor ensures that for background sources with redshifts much higher than the targeted cluster, the contribution to the rotation of the polarization angle from the vicinity of the radio source will be negligible (unless that RM contribution is extremely high), since it occurs at much higher frequencies. RM is related to the thermal electron density, n_e (cm^{-3}), and the line-of-sight magnetic field, B (μG), as

$$\text{RM} = 812 \int_0^L n_e B \cdot \text{d}l \ \text{rad m}^{-2}, \tag{2}$$

where the path-length dl is measured in kpc.

The rotation measure has contributions from all along the line of sight, from the intergalactic medium (IGM) in the vicinity of the source itself, from the intracluster medium (ICM) in the clusters along the line of sight, and from our own Galaxy. The galactic contribution typically dominates at Galactic latitudes below about $|b| < 20°$. Above $|b| > 40°$, the Galactic contribution becomes smaller than $|\text{RM}| < 30$ rad m^{-2} (Simard-Normandin & Kronberg 1980), and can be as small as 5 rad m^{-2} (Guidetti et al. 2008). Hence, high rotation measure from extragalactic sources at high Galactic latitudes can most likely be attributed to Faraday rotation within the gas in galaxy clusters.

1.1 Observations to date

So far, the only individual cluster with a significant number of observed polarized members and background sources is the Coma cluster. Seven sources within 35 arcmin display a clearly enhanced $|\text{RM}|$ between 35 and 65 rad m^{-2} (Kim et al. 1990; Feretti et al. 1995). These sources, as well as control sources in the vicinity of the cluster, but avoiding sightlines through Coma's ICM, have been observed in many individual pointings with the VLA. For the cluster A514, six embedded radio sources have been observed in individual VLA pointings. These show a decline of $|\text{RM}_{\text{max}}|$ from 154 rad m^{-2} in the centre of the cluster to 15 rad m^{-2} on the outskirts.

Table 1. Comparison of radio telescopes – derived properties.

Name	VLA[a]	SKA AA	SKA dishes	SKA dishes phase 1
$A_{\text{eff}}/T_{\text{sys}}$[b]	70–180	10 000	10 000	1200
Frequencies of interest (GHz)	0.3–0.34, 1.24–1.7, 4.5–5, 8.1–8.8	0.3–1	0.8–10	0.8–10
Instantaneous bandwidth (MHz)	86	700	250	250
1 h sensitivity (μJy)	17	0.18	0.29	2.5
Field of view (deg^2)[c]	$(0.7/f)^2$	250	2	20[d]

[a]See http://www.vla.nrao.edu/astro/guides/vlas/current/.
[b]Effective collecting area over system temperature.
[c]For the dish telescopes, given at the bottom of the frequency range; f denotes the observing frequency in GHz.
[d]Assuming phased array feeds.

Several other clusters, each with a few polarized sources, have been observed with similar results (Feretti et al. 1999; Taylor et al. 2001; Govoni et al. 2006; Guidetti et al. 2008). Many clusters have only one or two sufficiently bright radio sources in or behind them.[1] Therefore, stacking has been used to infer a general RM value for nearby clusters (Clarke et al. 2001). A systematic increase in |RM| is found towards the cluster cores.

First attempts have been made to infer the magnetic field structure via the power-spectrum with Faraday rotation studies. For the cluster A2255, Govoni et al. (2006) measure the Faraday rotation of four embedded radio sources. For different assumptions about the magnetic field power spectrum, they can extrapolate these data to predict the synchrotron emission of the radio halo. Comparison to observations of the radio halo then constrains the power-law index of the magnetic field's three-dimensional power spectrum to the range of three to four, consistent with Kolmogorov turbulence, with a possible spatial variation. The model also predicts polarization of the halo, which is indeed detected.

This paper is structured as follows: first, we discuss the simulation method in Section 2. The Faraday rotation detection statistics and the implications for the measurement of the cosmological evolution of the magnetic field in clusters are presented in Section 3. We discuss our findings in Section 4 and summarize them in Section 5. Throughout, we use the following cosmological parameters: $h = 0.7$, $\Omega_m = 0.3$, $\Omega_\Lambda = 0.7$.

2 THE SIMULATIONS

In order to assess the effect of cluster Faraday screens on the polarization of background radio sources, a relatively sophisticated model of clusters and source populations is required.

2.1 Cluster model

In order to model the cluster number within an observed patch of sky (here 10 deg^2), we require a model for the cosmologically evolving cluster mass function. For this, we employ a cluster mass function whose multiplicity function (see e.g. Sheth & Tormen 1999) is based on a moving barrier shape ansatz and depends on a minimal number of parameters to provide a suitable fit to numerical simulations. In particular, the shape of the used mass function has been derived from *N*-body simulations of large cosmological volumes and high resolutions following the method described in Jenkins et al. (2001). The above model gives the cluster mass function as a function of redshift. We adopt a lower mass cut-off of 3×10^{13} M$_\odot$ and for a given realization of the sky model derive cluster counts as a function of redshift, making allowance for cosmic variance. Our resulting galaxy cluster catalogue contains 775 objects, with redshifts up to ~ 2.3. The properties of our generated galaxy cluster sample are illustrated in Fig. 1.

In our model, clusters are distributed randomly and radio sources are either background or foreground objects with respect to a given cluster. Every object is placed on a 3D grid, covering $\sqrt{10} \times \sqrt{10}$ deg^2 and the redshift space from zero to eight. The spatial resolution is 6000×6000 cells, and redshift space is covered by 240 cells. This gives an effective resolution of 1.9 arcsec and d $z = 0.033$ in the third dimension.
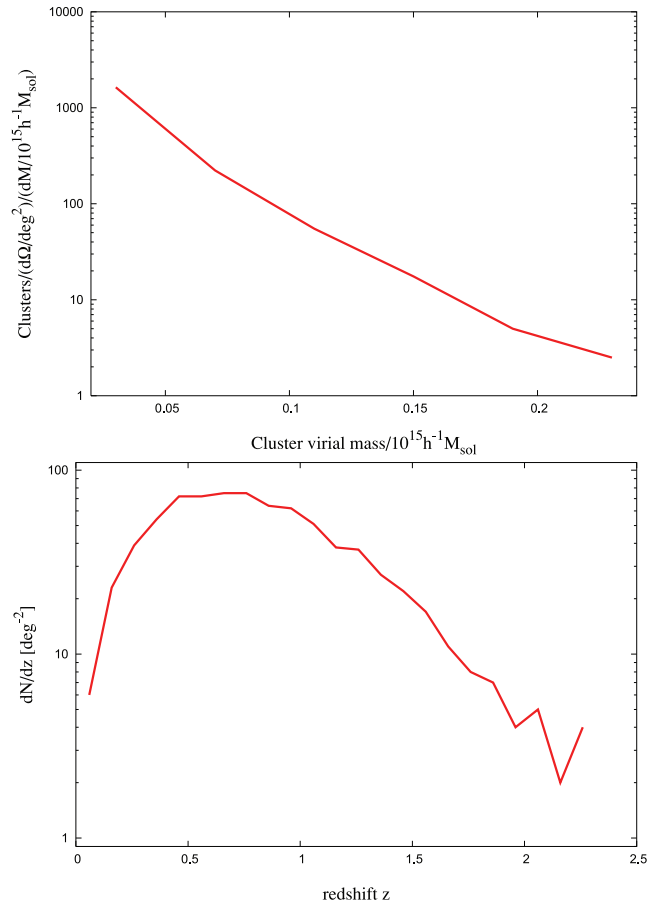
[1] See http://www.mpa-garching.mpg.de/~kdolag/BCluster/.

Figure 1. Mass (top panel) and redshift (bottom panel) distribution of the adopted galaxy cluster model. See text for details of the model.

2.2 Rotation measure model

The observational data on the structure of magnetic fields in clusters is currently sparse. Based on Clarke et al. (2001), we therefore employ a simple model for the rotation measure, with a peak value (justified in Section 2.9 below) drawn from a uniform random distribution between RM$_0 = \pm 5000$ rad m^{-2}, and a decline according to a β-model:

$$\mathrm{RM}(r) = \mathrm{RM}_0 \left(1 + r^2/r_0^2\right)^{-3\beta_{\mathrm{RM}}/2}. \tag{3}$$

We use $\beta_{\mathrm{RM}} = 1$ (see below) and $r_0 = 0.0636\, r_{200}$ (Biviano & Salucci 2006), where r_{200} is the radius within which there is an overdensity of a factor 200 compared to the mean density of the Universe at the redshift of the cluster. r_{200} is roughly equal to the virial radius of the cluster. This results in core radii between 20 and 110 kpc, which corresponds to angular sizes between a few arcseconds to half an arcminute.

Biviano & Salucci (2006) give a value of $\beta = 2/3$ for the gas density distribution in clusters of galaxies. The temperature distribution in clusters of galaxies is typically not far from isothermal (except in the centres of cool core clusters). Therefore, the pressure follows a very similar radial profile as that of the density. Equipartition between the magnetic and the thermal pressure is probably a reasonable assumption for the magnetic field distribution in clusters, and consistent with some RM data (e.g. Govoni et al. 2006; Guidetti et al. 2008). Consequently, we adopt a value of $\beta_{\mathrm{m}} = 1/3$ for the radial distribution of the magnetic field strength along the line of sight. The line-of-sight integral then results in the β-model for the

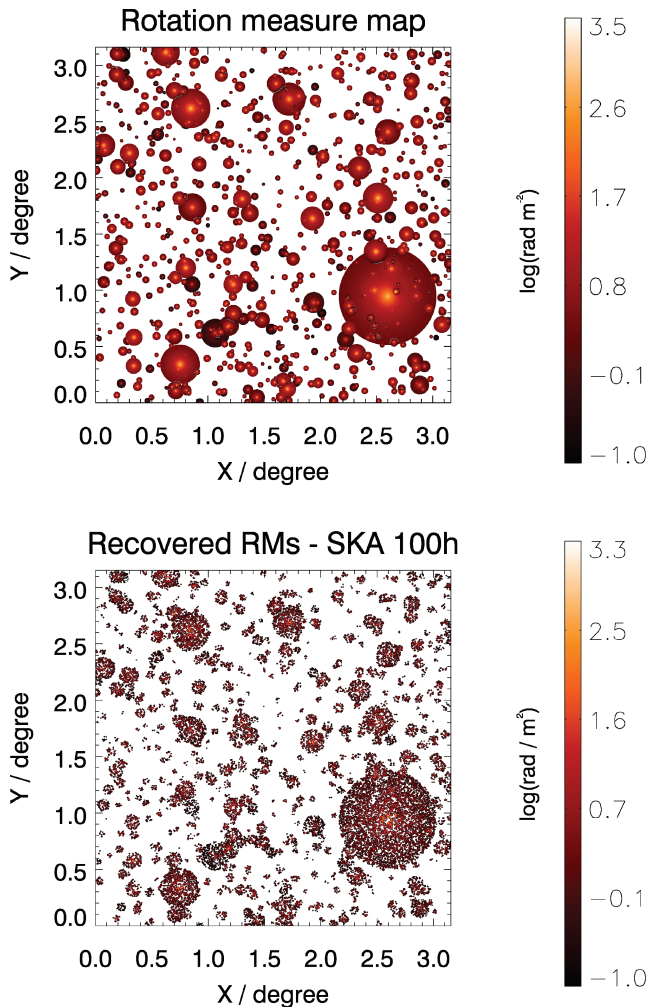## Rotation measure map

Recovered RMs - SKA 100h

Figure 2. Top panel: derived distribution of cosmological rotation measures on the sky due to galaxy clusters. Bottom panel: recovered RM sky due to background radio sources for a 100 h SKA AA observation. To enhance contrast, the resolution has been reduced by a factor of 10 compared to the figure on the top. The real field of view as planned to date would be 25 times larger.

rotation measure described in equation (3) above, with $\beta_{RM} = 1$. We calculate the rotation measure contribution out to the virial radius.

We show in Fig. 2 (top) the resulting distribution of rotation measures due to the simulated galaxy clusters. Much of the sky is covered with galaxy clusters, however, many of the systems have small rotation measures. About 12 per cent of the sky is covered with regions of at least 10 rad m^{-2}. The fraction reduces by a factor of about 2 if one considers rotation measures above 20 rad m^{-2}. In our chosen cosmology, only 34 per cent of all clusters are located beyond a redshift of one. These are obviously smaller on average than the lower redshift population. Hence, essentially all of the area coverage happens up to a redshift of unity (Fig. 3). Therefore, up to this redshift, structure determination should be much easier than beyond.

2.3 Radio source model

To obtain realistic models of the radio source populations, we use the publicly available Square Kilometre Array European Design Study (SKADS) synthetic radio source catalogue (SKADS simu-
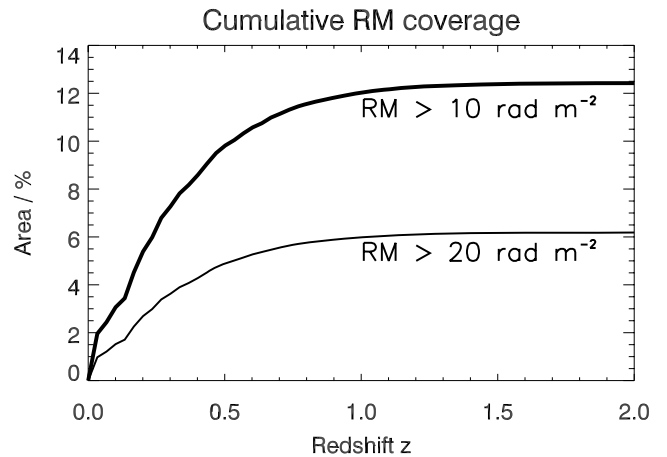
Cumulative RM coverage

Figure 3. Fraction of sky covered with RM > 10 rad m^{-2} (upper curve) and RM > 20 rad m^{-2} (lower curve).

lated skies, S^3; Wilman et al. 2008).[2] The catalogue is derived from semi-empirical simulations of different populations of radio continuum sources and extends down to faint flux limits in order to allow observation simulations of high-sensitive future radio telescopes, such as the SKA. The source populations included in the catalogue are radio-loud (FR I and FR II) and radio-quiet active galactic nuclei (AGNs) as well as radio emitting starburst and normal disc galaxies. The luminosity function corresponding to each class of sources is derived empirically from available observations. The fits are extrapolated to low luminosities and assume redshift evolutions to assure the simulations are complete down to the instrumentally expected (faint) flux limits. Our version of the catalogue covers 10 deg^2 of sky out to a redshift of eight with a 1.4 GHz flux limit of 1 μJy in Stokes *I*. See Wilman et al. (2008) for a detailed description of the radio source simulations.

2.4 Polarization model

The degree of polarization has to be determined for individual sources. We base our prediction of the polarization of these radio sources on the statistics of the National Radio Astronomy Observatory (NRAO) VLA Sky Survey (NVSS) catalogue (Condon et al. 1998). Tucci et al. (2003) have analysed polarization statistics from the NVSS and other sources in detail. Depending on spectral shape and source flux, they derive median fractional polarizations between 1.12 and 1.77 per cent for NVSS sources. For the NVSS (1.4 GHz), the probability distribution of the fractional polarization declines monotonically, but for higher observing frequencies, a turnover may be seen towards lower fractional polarization. This is due to a systematic increase of the fractional polarization with observing frequency. Tucci et al. (2003) explain these findings by Faraday depolarization. Therefore, we expect that the low-frequency distribution function also turns over at a not yet measured fractional polarization. We, therefore, fit a lognormal function to the measured part of the fractional polarization distribution function at 1.4 GHz. This results in a median value of 1.64 per cent and a standard deviation of 0.7 per cent. Tucci et al. (2003) believe that some of the NVSS sources are depolarized by differential Faraday rotation in intervening galaxy clusters. We argue that this would be much less so for SKA observations: the main reason is that with

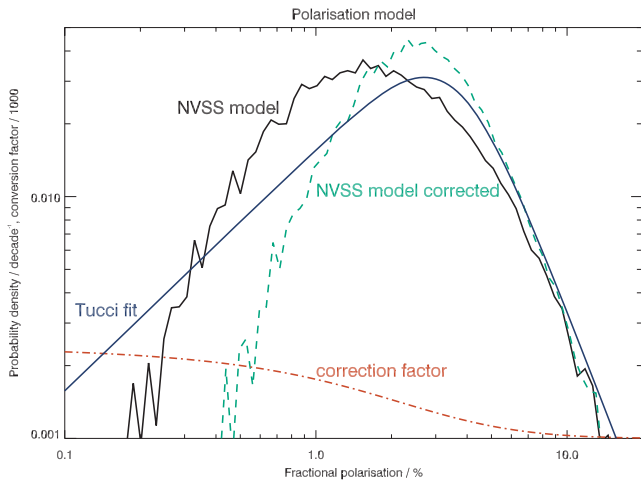[2] See http://s-cubed.physics.ox.ac.uk/.

Figure 4. Distribution of the fractional polarization for the radio source model. The dark blue smooth line represents the fit from Tucci et al. (2003) (not yet corrected for Faraday depolarization). The solid black line represents our adaptation of this fit. This model is corrected for Faraday depolarization by the polarization dependent correction factor shown as red dot–dashed curve (divided by 1000). The model finally adopted in this paper is shown as a green dashed line. The polarization distribution functions agree all at high fractional polarizations, were they are gauged against NVSS data.

lower flux limit, the radio source population changes. Extended jet sources dominate at high flux densities, and star forming galaxies at increasing distance and decreasing angular size at lower flux densities. For high-redshift galaxy clusters, the depolarization frequency is reduced by a factor $(1 + z)^{-1}$. Extended sources behind nearby clusters will be much better resolved than by the NVSS (45 arcsec). For a turbulent power spectrum, the RM variations should have less power on smaller scales, hence the depolarization frequency will be lower (Krause, Alexander & Bolton 2007).

For these reasons, we adopt the de-depolarization model from Tucci et al. (2003) to derive the intrinsic polarization Π from the potentially Faraday depolarized polarization Π_{FD}, that is drawn from a random distribution as described above:

$$\Pi = \Pi_{\mathrm{FD}} f(\Pi_{\mathrm{FD}}, \nu_{\mathrm{GHz}})/f(\Pi_{\mathrm{FD}}, 1.4)$$

$$f(p, \nu) = 72 \log(0.5\nu^{0.4} + 0.75) \exp(-3.2p^{0.35} + 0.8). \qquad (4)$$

Here, ν_{GHz} is a reference frequency in GHz. We use 10 GHz as the reference frequency, assuming that Faraday depolarization for NVSS sources mainly occurs below 10 GHz. The correction increases the fractional polarization by a factor of about 2, for those sources with low polarization at 1.4 GHz, as shown in Fig. 4. This effect has been measured already: Taylor et al. (2007) measure an increase of the fractional polarization downwards of 100 mJy of a factor of 3 compared to the high flux density sources, in agreement with the model we propose.

2.5 Redshift distribution

For decreasing flux limit, the radio source counts are dominated by sources of increasing redshift. We show the redshift distribution for different (polarized) flux limited samples in Fig. 5. For a polarized flux-density of 100 μJy, roughly the level of current studies (Taylor et al. 2007), the median redshift is 0.6. It rises to 1.3 for a polarized flux limit of 0.1 μJy, appropriate for a 100 h SKA observation. Even for the highest redshifts, we still predict thousands of background sources per square degree for this flux limit.
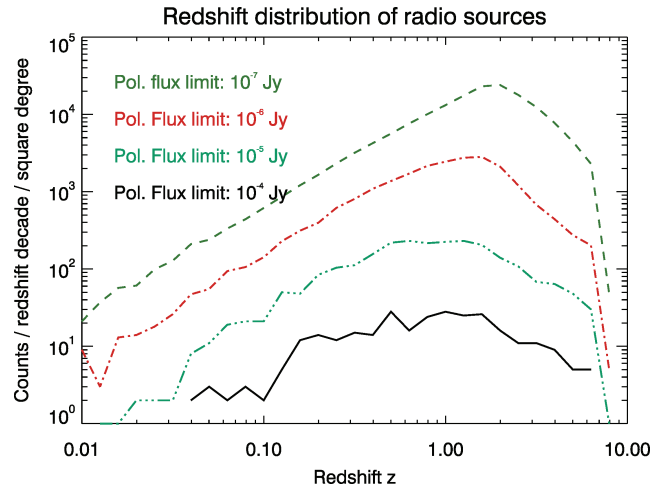

Figure 5. Distribution of radio sources against redshift for different polarized flux limits. From top to bottom, the curves represent: 0.1, 1, 10 and 100 μJy. The median redshift is 0.6, 0.6, 0.8 and 1.3.

2.6 Required signal-to-noise ratio for RM measurements

A distinctive feature of the next generation of radio telescopes is that a large bandwidth and high spectral resolution will be available simultaneously. Rotation measure synthesis is an established technique to analyse RM data. However, for the analysis of the RM-grid, we wish to extract information from the faintest detectable sources. For the faintest sources we will extract a single value of the rotation measure. Here, we consider the minimum signal-to-noise ratio (SNR) on a point source required for this. Faraday rotation leads to sinusoidal variation with respect to λ^2 across the band for the Stokes parameters Q and U, modulated by a function giving the fractional polarization as a function of wavelength and the intrinsic spectrum of the source. We consider normalized Stokes parameters:

$$\begin{pmatrix} Q' \\ U' \end{pmatrix} = (Q^2 + U^2)^{-1/2} \begin{pmatrix} Q \\ U \end{pmatrix},$$

$$= \begin{pmatrix} \cos(2\mathrm{PA} + 2\mathrm{RM}\lambda^2) \\ \sin(2\mathrm{PA} + 2\mathrm{RM}\lambda^2) \end{pmatrix}, \qquad (5)$$

where Q and U are the ordinary Stokes parameters. To assess the required SNR, required of a background source to measure a given foreground RM, we perform Monte Carlo simulations. Our simulated data were for a background source with a spectral index of 0.7 – we simulate the observing band, taking a constant channel width of $\Delta\nu = 1$ MHz. We perform a combined χ^2 fit to the normalized Stokes parameters, and use the flux at 1.4 GHz as a reference point for the SNR. For infinite SNR, the minimization of χ^2 would be straight forward. For decreasing SNR, additional minima appear in χ^2 as a function of RM. For a SNR of 10 (100), the distance between these minima is of the order of 1 rad m^{-2} (100 rad m^{-2}). A dense grid of starting guesses is, therefore, essential for a gradient search method to find the global minimum. The actual values of χ^2 differ only by a few percent, with the exception of the χ^2 for the true RM, and its negative. We find that χ^2 for the true RM and its negative are significantly lower than all other RMs (five times the standard deviation for 400 starting guesses) for an SNR of four and higher.

The sign ambiguity is due to the symmetry properties of the trigonometric functions. If a set (PA, RM), where PA is the high frequency polarization angle (compare equation 5), are the correct parameters to describe both functions, Q'(PA, RM) and U'(PA,

RM), then $(\pi + \text{PA}, -\text{RM})$ will be another solution regarding Q' and $(-\text{PA}, -\text{RM})$, respectively, for U':

$$Q'(\text{PA}, \text{RM}) = Q'(\pi + \text{PA}, -\text{RM}),$$

$$U'(\text{PA}, \text{RM}) = U'(-\text{PA}, -\text{RM}).$$

To fix the sign at low SNR, for each set of fitted parameters for Q', we also performed two fits for U' with starting guesses of $(\pi - \text{PA}, \text{RM})$ and (PA, RM), respectively, allowing only RM to vary, i.e. keeping the high-frequency polarization angle fixed. If the fit with (PA, RM) leads to the lowest minimum of χ^2, then we have found the correct RM. However, if the fit with $(\pi\text{-PA}, \text{RM})$ produces the lowest minimum of χ^2, then $-\text{RM}$ will be the correct rotation measure. The procedure is then repeated with U' and Q' exchanged. We may thus produce a combined χ^2 for RM and $-\text{RM}$. Selecting on the combined χ^2, we are able to recover the correct sign.

For RMs between 3 and 3000 rad m^{-2}, we find a minimum SNR between 4 and 10. This is true for the observing bands from 800 to 1050 MHz as well as 300 to 1000 MHz. In the following, we assume that a RM measurement may be done for any source detected at an SNR of 10 in polarized flux.

2.7 Rotation measure grid

For observations of nearby clusters, as well as the Galaxy, it is useful to compute the root-area-average distance between polarized background sources. Fig. 6 shows the average grid spacing over observing time for the adopted SKA and SKA phase 1 sensitivities. We use the point source sensitivity limit according to Wrobel & Walker (1999):

$$\mathrm{d}s = \frac{k_\mathrm{B} T_\mathrm{sys}}{\sqrt{2 \, \mathrm{d}\nu \, \tau} \, A \, \epsilon}, \tag{6}$$

where, k_B is Boltzmann's constant, T_sys is the telescope's system temperature, A the total effective area, $\mathrm{d}\nu$ the bandwidth, τ the observing time and ϵ the overall efficiency. Adopting a SNR of 10, we count the sources above the sensitivity limit for a particular telescope and observing time. The total source counts are roughly inversely proportional to the polarized flux, which is an effect of the adding up of the contributions from different source types. So, while the galaxies constitute the majority of the sources at low fluxes, other source types still contribute enough to flatten the overall distribution considerably.
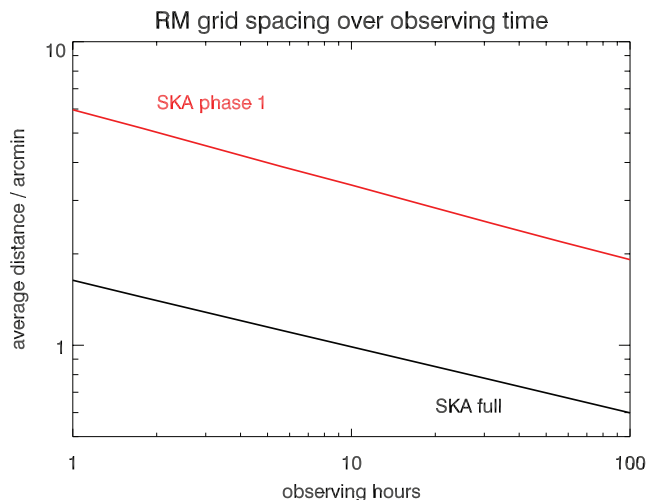

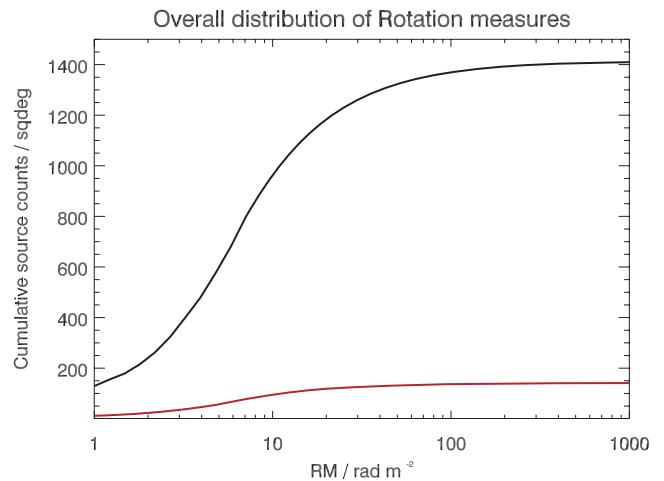**Figure 6.** RM grid spacing for different telescopes and a SNR of 10.

Figure 7. Cumulative histogram of all the rotation measures we expect to find within 1 deg^2 for a polarized flux limit of 1 μJy (lower red curve) and 0.1 μJy (upper black curve). In any case, we expect most of the measurements to yield rotation measures of the order of 10 to 100 rad m^{-2}.

2.8 Expected RM values

For each background source, we calculate the observed rotation measure by integrating through the simulation volume from the observed source to the observer. We show the cumulative histogram of all the rotation measures produced in this way in Fig. 7. We find that the majority of rotation measures are in the range 10–100 rad m^{-2}, due to the fact that most of the area comes from the outskirts of the clusters. The highest rotation measures come of course from the cluster centres. For a given frequency band and rotation measure range, a particular SNR is required. As shown above in Section 2.6, both of the frequency ranges, 300 to 1000 MHz (aperture array) and 800 to 1050 MHz (dish array), should be suitable for the great majority of expected rotation measures.

2.9 Core rotation measures

For each radio source within three virial radii of a given cluster centre, we also calculate the respective impact parameter, i.e. the projected distance to the cluster centre. We show these rotation measures against the impact parameter, for low redshift ($z < 0.5$), high mass ($M > 10^{14} \, \mathrm{M}_\odot$) clusters and a polarized flux limit of 1 μJy in Fig. 8. These cuts were employed in Clarke et al. (2001), and their data is also shown in Fig. 8. But our model and the observational data show only RM values up to $|\text{RM}| < 300 \, \text{rad m}^{-2}$, whereas our model has peak values of 5000 rad m^{-2} in the cluster centres. The reason is that at the high flux cut adopted here, the RM-grid is still very sparse, and hardly any source is located within the core radius. If we employ a lower central RM, with the same cuts, the simulated RM spread on the scale of the virial radius would be too small compared to the observed data. As can be seen, the central rotation measures of about 5000 rad m^{-2} that are used in the simulated data here are necessary to reproduce the observed spread of rotation measures. For distances greater than 1000 kpc and random sightlines, we encounter high RMs from neighbouring clusters. These are not present in Clarke et al. (2001), as they select their control sample avoiding known X-ray clusters.
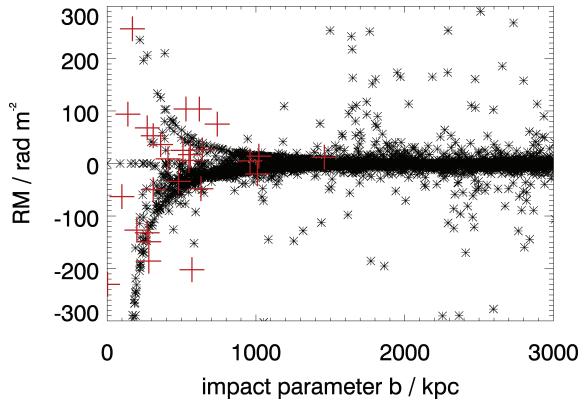
Figure 8. Rotation measure against impact parameter. The impact parameter is the projected distance of a radio source to a given cluster centre. Low-redshift ($z < 0.5$), high-mass ($M > 10^{14}\,\mathrm{M_\odot}$) clusters have been selected in order to compare to the observed data of Clarke et al. (2001). The polarized flux limit is 1 μJy, as in Clarke et al. (2001). Observational data from Clarke et al. (2001) (cluster sample only) is provided as red crosses. For distances greater than 1000 kpc, the sightlines to the radio sources pierce neighbouring clusters. To get the observed RM spread at the observed impact parameters, central RMs of about 5000 rad m^{-2} are necessary.

3 RESULTS

3.1 Detection statistics

We show the detection statistics for the SKA aperture array and the phase 1 SKA in Fig. 9 and Table 2. The histograms demonstrate the progress that can be expected from the SKA, especially the full aperture array.

For a one hour phase 1 dish blind survey, we predict to find 30, 214 and 148 clusters in the redshift ranges 0–0.2, 0.2–0.5, 0.5–1, respectively, with at least one background RM measurement, each. We also predict a few detections at higher redshift. This would allow stacking experiments for different redshift bins out to a redshift of at least one. Also, one could determine the decline of the average RM with cluster radius better than presently possible. This could answer the question whether the magnetic field energy density follows the thermal energy density. We also would have some chance to find about a couple of nearby clusters with 30–100 RMs, allowing an improved determination of the field structure. 30 background sources should be enough to constrain the power spectrum (Govoni et al. 2006; Guidetti et al. 2008). Since the positions of the big nearby clusters are known, a targeted survey would certainly yield about this number of RMs.

A 100 h phase 1 observation would result in 26 clusters at $z < 0.5$ with more than 30 background sources, and a couple of these having more than 300 background sources. This would allow to study the field structure in some detail. Up to a redshift of unity, nearly every cluster in the field of view should have at least one background source. Even beyond $z = 1$, we predict to find 490 clusters with one to several background sources. This would allow the extension of the stacking method to this redshift.

The full SKA aperture array will finally allow to measure the structure of the magnetic field in great detail: even for a 1 h observation, each low-redshift cluster will at least have 10 background sources, 25 of which over 300. We predict to find 325 clusters in total with more than 30 background sources, distributed over a redshift range of up to 0.5, promising good statistics of the variance of the power spectrum from cluster to cluster. More than 10 000 clus-

ters would be detected with at least one RM measurement beyond a redshift of 0.5.

For a 100 h pointing, we will be able to constrain the power spectrum for many clusters in the field of view up to a redshift of one (>5000 clusters with more than 30 background sources). Up to a redshift of one, we expect >1000 clusters with at least 100 RMs. Only for such clusters, we may expect to *resolve* the core in some cases, i.e. to have at least one background source within the cluster's core radius. A 100 h pointing would correspond roughly to the sensitivity limit used in Fig. 10, where we show the decrease of the maximum rotation measure in any given cluster with redshift due to the decreased likelihood to get a background source within the core radius. 25 clusters should have more than 1000 background sources, and hence allow a very detailed determination of the magnetic field structure, even in the cluster cores.

Due to the limited field of view, the full SKA dish array would not nearly reach the detection rates of the aperture array. Even a 100 h blind survey would only yield 24 clusters with more than 30 background sources.

3.2 Cosmological evolution

Clusters at higher redshift cover less area of sky (up to a redshift of 1.6). Also, there are fewer sources behind a unit area at higher redshift. Therefore, the probability that a cluster centre has a background object decreases as the redshift increases. We plot the maximum rotation measure that we detect for a polarized flux limit of 0.1 μJy against any given cluster versus the cluster redshift in Fig. 10. Out to a redshift of unity, there is still a good chance of finding sightlines through the cluster core. However, the median maximum rotation measure decreases by almost a factor of 4 for clusters with redshift 0.5–1 compared to ones at 0–0.5. The decrease in the median of the measured maximum rotation measure is almost exponential with redshift, with an 1/e-decay length in z close to 0.4. We can check the detectability of possible trends with redshift by multiplying the rotation measures with $(1 + z)^n$ where we have chosen n to be ± 1 as example. The change in the median rotation measure is also indicated in Fig. 10. The decay length changes to 0.3 and 0.5, respectively. If we compare the redshift intervals 0–0.5 and 0.5–1, we predict a decrease of the median rotation measure by factors of about 3, 4 and 5, respectively (compare with Table 3, which is normalized to the low-redshift value).

The statistical error on the median maximum rotation measure is given by

$$\sigma_M = 1.253\sigma/\sqrt{N},$$

where σ is the standard deviation and N is the number of sources in the respective bin. We have calculated the median maximum RM for any given cluster and the statistical errors for a 100 h SKA AA observation for different values of n. This is shown in Table 3. Differences in the exponent n of 0.3 could be distinguished.

4 DISCUSSION

We assess the capability of the SKA and its precursor, phase 1 SKA, to detect rotation measures and determine the evolution of magnetic fields in galaxy clusters. Our cluster and radio source simulations are based on standard cosmological methods and extrapolation of available observational data. We use a fractional polarization model based on NVSS data, moderately corrected for Faraday depolarization, at low fractional polarizations, only.
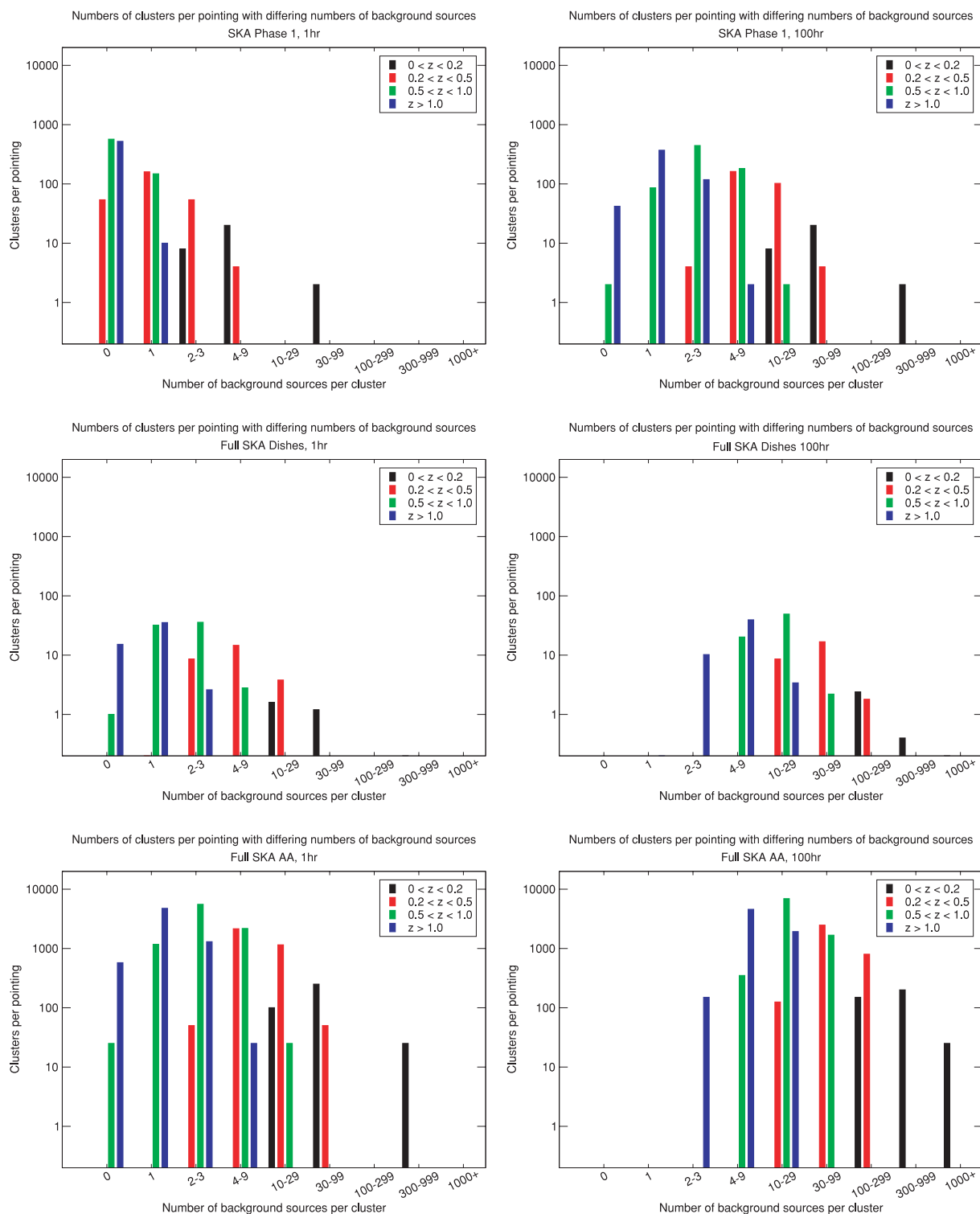
Figure 9. Detection statistics for the SKA aperture array (bottom row), the full SKA dish array (middle row) and the phase 1 SKA dish array (top row), telescope specs from Table 1, for an observing time of 1 h (left) and 100 h (right), respectively. We plot the number of background sources per cluster on the horizontal axis, and the cluster counts for the particular bins on the vertical axis. The huge number counts found with the full SKA aperture array is a merit of its huge field of view (250 deg^2) combined with its high sensitivity. The same information is provided in tabular form in Table 2.

We find that about 10 per cent of the whole sky should be covered with rotation measures greater than 10 rad m^{-2}. If the cosmology is known, this may serve as an additional constraint to check for the proper removal of the Milky Way's RM foreground. Large clusters can have an RM contribution from background clusters. However, the contamination occurs mainly on the outskirts of these clusters.

Our simulations show that core RMs of about 5000 rad m^{-2} are necessary to explain the currently known stacking data, which

Table 2. Cluster counts with a given number of background sources.

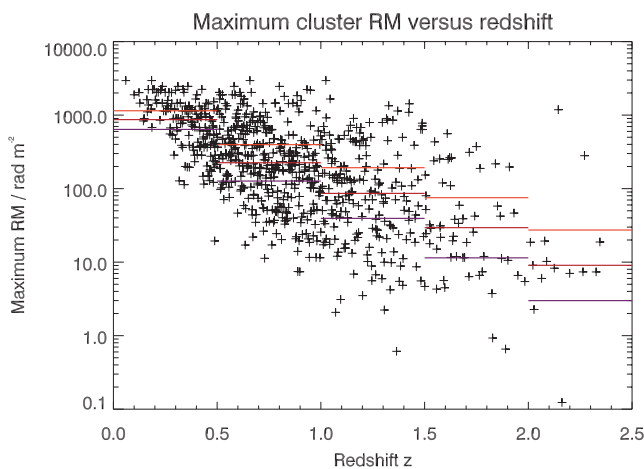| Redshift interval	Number of polarized background sources per cluster								
	0	1	2–3	4–9	10–29	30–100	100–299	300–999	1000+
Phase 1 dishes, 1 h pointing									
0–0.2	0	0	8	20	0	2	0	0	0
0.2–0.5	54	160	54	0	0	0	0	0	0
0.5–1	568	148	0	0	0	0	0	0	0
>1	522	10	0	0	0	0	0	0	0
Phase 1 dishes, 100 h pointing									
0–0.2	0	0	0	0	8	20	0	2	0
0.2–0.5	0	0	4	162	102	4	0	0	0
0.5–1	2	86	444	182	2	0	0	0	0
>1	42	370	118	2	0	0	0	0	0
Full SKA dishes, 1 h pointing									
0–0.2	0	0	0	0	1.6	1.2	0	0.2	0
0.2–0.5	0	0.2	8.6	14.6	3.8	0	0	0	0
0.5–1	1	32	35.8	2.8	0	0	0	0	0
>1	15.2	35.4	2.6	0	0	0	0	0	0
Full SKA dishes, 100 h pointing									
0–0.2	0	0	0	0	0	0	2.4	0.4	0.2
0.2–0.5	0	0	0	0	8.6	16.8	1.8	0	0
0.5–1	0	0	0	20.2	49.2	2.2	0	0	0
>1	0	0.2	10.2	39.4	3.4	0	0	0	0
Full SKA AA, 1 h pointing									
0–0.2	0	0	0	0	100	250	0	25	0
0.2–0.5	0	0	50	2150	1150	50	0	0	0
0.5–1	25	1175	5550	2175	25	0	0	0	0
>1	575	4750	1300	25	0	0	0	0	0
Full SKA AA, 100 h pointing									
0–0.2	0	0	0	0	0	0	150	200	25
0.2–0.5	0	0	0	0	125	2475	800	0	0
0.5–1	0	0	0	350	6925	1675	0	0	0
>1	0	0	150	4575	1925	0	0	0	0

Figure 10. Maximum rotation measure seen against any given cluster in our sample against cluster redshift for a polarized flux limit of 0.1 μJy. The red lines denote the median for subsamples with corresponding redshifts (0–0.5, 0.5–1, 1–1.5, 1.5–2, >2). The purple lines denote the measured rotation measures if the true rotation measures would decline with redshift as $(1 + z)^{-1}$, the orange line displays the medians for an increase proportional to $(1 + z)$.

shows about 200 rad m^{-2} on the scale of the virial radius. RMs against central cluster radio sources often reach values comparable to our core RMs (Carilli & Taylor 2002). This suggests that our assumption for the core RMs is realistic, but also that the functional form of the radial decline we assume is not too far from reality.

How would the derived statistics change if one were to change the radial RM profile? The adopted profile has high core values with a steep decline. With this distribution, we have shown to match the observations of nearby clusters. However, one might argue that these nearby clusters may not be representative of the whole cluster population. One might imagine that a less centrally peaked flatter distribution, like, for example, in the Coma cluster, might be more typical. We have shown in Section 2.6 that the optimum RM range is between a few and a several 100 rad m^{-2}. Such a scenario would, therefore, lead to an increase of the fraction of sky in our best range. Therefore, the RM distribution we have chosen is, if anything, rather pessimistic.

We show that with a phase 1 SKA, as defined in Table 1, good stacking experiments should be possible, determining the average magnetic field profile locally and also out to a redshift of about one. The field structure should be measurable for some nearby clusters. If there would be a choice necessary between a deep survey and 100 one hour pointings, one should probably do the deep survey,

Table 3. Median maximum rotation measure in any given cluster against redshift for different assumptions about the intrinsic evolution, where n is the exponent for a systematic change with redshift. The statistical errors are applicable for a 100 h SKA AA observation. The values in each row have been normalized to the lowest redshift bin.

n	$z = 0$–0.5	$z = 0.5$–1	$z = 1$–1.5	$z = 1.5$–2	$z > 2$
1	1 ± 0.015	0.346 ± 0.010	0.168 ± 0.012	0.066 ± 0.009	0.024 ± 0.058
0.5	1 ± 0.015	0.298 ± 0.009	0.128 ± 0.009	0.047 ± 0.007	0.016 ± 0.038
0.2	1 ± 0.015	0.276 ± 0.008	0.109 ± 0.007	0.039 ± 0.005	0.012 ± 0.029
0	1 ± 0.015	0.259 ± 0.008	0.099 ± 0.007	0.034 ± 0.005	0.010 ± 0.024

since it already allows some field structure determination in nearby clusters, and promises to measure RMs for clusters with $z > 1$.

With the full SKA AA aperture array, both a shallow 100 one hour pointing survey, and a deep survey promise very interesting results. A shallow 100 times one hour survey should detect RMs from about 10^6 clusters, with complete redshift coverage. A deep 100 h one field survey will allow structure determination in unprecedented detail out to a redshift of one: over 1000 clusters will have more than 100 RM measurements, 25 of which over 1000 RMs. The result of a 100 h deep survey is also shown graphically in Fig. 2 (bottom). To some extent, the two approaches are complementary: the 100 h deep survey would offer a complete RM survey for all structures above 3×10^{13} M$_\odot$, and thereby exclude possible selection biases which could arise if only a fraction of the clusters is detected as in the shallow survey. The shallow survey would be able to detect large-scale bias, and also would provide better overall statistics on the cosmological field evolution, if details within the clusters are neglected.

Without phased array feeds on the majority of the dishes, as assumed here, the detection rates remain rather small for the full SKA dish array. However, having similar sensitivity than the aperture array, but coverage at higher frequencies, it would be a valuable complement for high RM regions (cluster centres), where the frequencies accessible to the aperture array would be depolarized. The RM grid density would be similar to the aperture array.

With the deep survey, we could measure the cosmic evolution of the RMs in clusters. If RM is proportional to $(1 + z)^n$, we could measure n to an accuracy of $\Delta n = 0.3$. In order to determine the evolution of the magnetic field from this, one needs additional information on the electron densities. If we would adopt an accuracy for n of $\Delta n = 0.3$, and assume a similar behaviour and accuracy for the electron densities, to be measured via the Sunyaev–Zel'dovich effect (Sehgal, Kosowsky & Holder 2005), we would end up with an accuracy for a power-law index for the magnetic field [$B \propto (1 + z)^m$] of 0.4. This should be regarded as a conservative estimate, since it only takes into account information from the deep survey. Additional information from a shallow survey should improve the accuracy for the low-redshift bins. Also, we have only used the information on the maximum RM per cluster. Taking into account the full data will also improve the statistics.

For a polarized flux limit of 0.1 μJy, as appropriate for a 100 h SKA pointing and an SNR of 10, we predict a few 10 000 radio sources per square degree. These sources have a broad redshift distribution, with a median redshift of about one, rising with decreasing flux limit. We can hence expect not only to find the reported numbers of background sources, but also a sizable number of foreground sources, of the order of a few percent of the background sources, rising of course with cluster redshift. An accurate determination of the foreground RM opens up the possibility to detect a possible small mean cluster RM which would point to a super-cluster scale

field connecting the cosmic web. This would be the first detection of such a field.

5 CONCLUSIONS

We have modelled the distribution of rotation measures for the SKA. We calculate the average distance between rotation measures to be between 6 arcmin for a 1 h observation with the early SKA and 36 arcsec for a 100 h pointing with the full SKA. We expect to find rotation measures mostly up to 100 rad m^{-2}, with the cluster centres reaching up to several thousand. The planned SKA mid-frequency aperture array (300–1000 MHz) as well as the lowest band of the dish array would be well suited for the great majority of sources. High RM cluster centres would require targeted high-frequency follow-up observations. We find that current Faraday rotation studies only represent the outskirts of galaxy clusters. The average RM should increase steadily towards the core to reach typically several thousand rad m^{-2}.

A phase 1 SKA would already improve the statistics for current stacking experiments considerably, and make this experiment viable out to redshifts $z > 1$. The full SKA aperture array would detect over a million clusters with at least one background source each in a shallow 100 h survey, and allow detailed field structure determination (>1000 clusters with more than 100 background sources each) with a deep survey. If the cosmological evolution of the rotation measures is proportional to $(1 + z)^n$, the SKA would be able to measure n to an accuracy of 0.3. Compared to the few RMs known for a few nearby clusters today, this will revolutionize our knowledge of rotation measures in galaxy clusters. Provided the electron densities can be measured via the Sunyaev–Zel'dovich effect at high redshift, we can expect to follow the build-up of cosmic magnetism with the SKA.

REFERENCES

Alexander P., Faulkner A., 2009, SKA Memo 108, http://www.skatelescope.org/
Bagchi J., Pislar V., Lima Neto G. B., 1998, MNRAS, 296, L23
Biviano A., Salucci P., 2006, A&A, 452, 75
Carilli C. L., Taylor G. B., 2002, ARA&A, 40, 319
Clarke T. E., Kronberg P. P., Böhringer H., 2001, ApJ, 547, L111
Condon J. J., Cotton W. D., Greisen E. W., Yin Q. F., Perley R. A., Taylor G. B., Broderick J. J., 1998, AJ, 115, 1693
Feretti L., Giovannini G., 2008, in Plionis M., López-Cruz O., Hughes D., eds, Lecture Notes in Physics, Vol. 740, A Pan-Chromatic View of

Clusters of Galaxies and the Large-Scale Structure. Springer, Dordrecht, p. 143

Feretti L., Dallacasa D., Giovannini G., Tagliani A., 1995, A&A, 302, 680

Feretti L., Dallacasa D., Govoni F., Giovannini G., Taylor G. B., Klein U., 1999, A&A, 344, 472

Giovannini G., Feretti L., Venturi T., Kim K.-T., Kronberg P. P., 1993, ApJ, 406, 399

Govoni F., Feretti L., 2004, Int. J. Mod. Phys. D, 13, 1549

Govoni F., Murgia M., Feretti L., Giovannini G., Dolag K., Taylor G. B., 2006, A&A, 460, 425

Guidetti D., Murgia M., Govoni F., Parma P., Gregorini L., de Ruiter H. R., Cameron R. A., Fanti R., 2008, A&A, 483, 699

Jenkins A., Frenk C. S., White S. D. M., Colberg J. M., Cole S., Evrard A. E., Couchman H. M. P., Yoshida N., 2001, MNRAS, 321, 372

Kaiser C. R., Binney J., 2003, MNRAS, 338, 837

Kim K.-T., Kronberg P. P., Dewdney P. E., Landecker T. L., 1990, ApJ, 355, 29

Kim K.-T., Kronberg P. P., Tribble P. C., 1991, ApJ, 379, 80

Krause M., Alexander P., Bolton R., 2007, in Proceedings of Science, From Planets to Dark Energy: the Modern Radio Universe, POS(MRU)109, http://pos.sissa.it/

Murgia M., Govoni F., Feretti L., Giovannini G., Dallacasa D., Fanti R., Taylor G. B., Dolag K., 2004, A&A, 424, 429

Schilizzi R. T. et al., 2007, SKA Memo 100, http://www.skatelescope.org/

Sehgal N., Kosowsky A., Holder G., 2005, ApJ, 635, 22

Sheth R. K., Tormen G., 1999, MNRAS, 308, 119

Simard-Normandin M., Kronberg P. P., 1980, ApJ, 242, 74

Taylor G. B., Govoni F., Allen S. W., Fabian A. C., 2001, MNRAS, 326, 2

Taylor A. R. et al., 2007, ApJ, 666, 201

Tucci M., Martínez-González E., Toffolatti L., González-Nuevo J., de Zotti G., 2003, New Astron. Rev., 47, 1135

Vogt C., Enßlin T. A., 2005, A&A, 434, 67

Wilman R. J. et al., 2008, MNRAS, 388, 1335

Wrobel J., Walker R., 1999, in Taylor G. B., Carilli C. L., Perley R. A., eds, ASP Conf. Ser. Vol. 180, Synthesis Imaging in Radio Astronomy II. Astron. Soc. Pac., San Francisco, p. 171

This paper has been typeset from a TEX/LATEX file prepared by the author.